Available online at www.sciencedirect.com
SCIENCE DIRECT®
International Journal of Heat and Mass Transfer 48 (2005) 4498–4509
International Journal of HEAT and MASS TRANSFER
www.elsevier.com/locate/ijhmt

An analytical model for fluid flow and heat transfer in a micro-heat pipe of polygonal shape

Balram Suman [a,b,*], Prabhat Kumar [c]

[a] Department of Chemical Engineering and Materials Science, Mailbox # 30, 151 Amundson Hall, 421 Washington Avenue, SE, University of Minnesota, Minneapolis 55455, MN, United States
[b] School of Mathematics, University of Minnesota, Minneapolis 55455, MN, United States
[c] Department of Food Science, North Carolina State University, Raleigh 27695, NC, United States

Received 18 January 2005; received in revised form 29 March 2005
Available online 11 July 2005

Abstract

An analytical model for fluid flow and heat transfer in a micro-heat pipe of polygonal shape is presented by utilizing a macroscopic approach. The coupled nonlinear governing equations for fluid flow, heat and mass transfer have been modified and have been solved analytically. The analytical model enables us to study the performance and the limitations of such a device and provides the analytical expressions for critical heat input, dry-out length and available capillary head for the flow of fluid. A dimensionless parameter, which plays an important role in predicting the performance of a micro-heat pipe, is obtained from the analytical model. The results predicted by the model compared with the published results in literature and good agreement has been obtained. The general and analytical nature of the simple model will have its applicability in the design of micro-heat pipes.

Keywords: Micro-heat pipe; Capillary forces; Critical heat input; Dry-out length; Analytical model

1. Introduction

Micro-grooved heat pipes have become one of the most promising cooling devices because of their high efficiency, reliability and cost effectiveness. The applications of micro-heat pipes have expanded from the thermal control of integrated electronic circuits packaging, laser diodes, photovoltaic cells, infrared (IR) detectors and space vehicles to the removal of heat from the leading edges of stator vanes in turbines and nonsurgical treatment of cancerous tissue. The current concepts in integrated circuit (IC) packaging are motivated by the development of metal oxide semi-conductor (MOS) and very large scale integration (VLSI) technologies, which require higher levels of device integration. The continuous increase in the device integration density leads to a rapid rise in the power generation from such device resulting in increased thermal gradient and higher mean operating temperature in the devices leading to their improper functioning. Thus, it is necessary to develop new thermal control schemes capable of removing heat from the electronic chip. In cases where large amounts of heat need to be removed, two-phase heat

* Corresponding author. Address: Department of Chemical Engineering and Materials Science, Mailbox # 30, 151 Amundson Hall, 421 Washington Avenue, SE, University of Minnesota, Minneapolis 55455, MN, United States. Tel.: +1 612 625 6083; fax: +1 612 626 7246.
E-mail address: suman@cems.umn.edu (B. Suman).

0017-9310/$ - see front matter © 2005 Elsevier Ltd. All rights reserved.
doi:10.1016/j.ijheatmasstransfer.2005.05.001

Nomenclature

a	side length of a regular polygon or smaller side of a rectangle, m
a_1	larger side length of a rectangle, m
A_{cs}	area of cross-section for fluid flow, m^2
A_l	total liquid area, m^2
A'_l	liquid area of one corner, m^2
B	performance factor
B_1	constant in expression for A_l
B'_1	constant in expression for R^* in condensing region
B'_2	constant in expression for R^* in adiabatic region
B'_3	constant in expression for R^* in evaporative region
B_2	constant in expression for $\frac{dR^*}{dX^*}$
f	friction factor
f_1	nondimensional coordinate of the junction of condensing and adiabatic sections
f_2	nondimensional coordinate of the junction of adiabatic and evaporative sections
g	acceleration due to gravity, m/s^2
K'	constant in expression for B_2
L	length of heat pipe, m
L_d	dry-out length, m
L_h	half of total wetted length, m
K_s	thermal conductivity, W/(m K)
m	constant in the expression for generalized heat flux
n	number of sides of a heat pipe polygon
N_{Re}	Reynolds number
P_l	liquid pressure, N/m^2
P^*_l	nondimensional liquid pressure
P_R	reference pressure, N/m^2
P_{vo}	pressure in vapor region, N/m^2
Q	net heat supplied, W
Q_{in}	heat input, W
Q'	heat input, W
Q'_c	heat flux in the condensing region, W/m^2
Q_{cr}	critical heat flux, W/m^2
Q'_e	heat flux in the evaporative region, W/m^2
Q_v	heat flux for vaporization of liquid, W/m^2
R	radius of curvature, m
R^*	nondimensional radius of curvature
R^*_1	nondimensional radius of curvature at f_1
R^*_2	nondimensional radius of curvature at f_2
R_0	reference radius, m
Re	rectangle
R_l	meniscus surface area per unit length, m
T_{con}	temperature at the cold end, °C
Tr	triangle
T_R	reference temperature, °C
T_s	temperature of substrate, °C
T^*_s	dimensionless substrate temperature
V_g	axial vapor velocity, m/s
V_l	axial liquid velocity, m/s
V^*_g	nondimensional vapor velocity
V^*_l	nondimensional liquid velocity
V_R	reference liquid velocity, m/s
W_b	perimeter of the heat pipe polygon, m
x	coordinate along the heat pipe, m
X^*	nondimensional coordinate along heat pipe
X^*_d	nondimensional coordinate of the onset of dry-region

Greek symbols

α	half apex angle of polygon, radian
β	inclination of substrate with horizontal, radian
γ	contact angle, radian
ϕ	curvature, m^{-1}
λ	latent heat of vaporization of coolant liquid, J/kg
μ	viscosity of coolant liquid, $kg\,m^{-1}\,sec^{-1}$
ρ_l	density of coolant liquid, kg/m^3
ρ_g	density of vapor, kg/m^3
σ	surface tension of coolant liquid, N/m
τ_w	wall shear stress, N/m^2
η, ξ, ζ	variables used for integration

Subscripts

c	condenser section
d	onset of dry-out region
e	evaporative section
g	vapor
l	coolant liquid

transfer can prove to be a better technique. Therefore, a micro-grooved heat pipe is one of the promising options for micro-electronics cooling. Although the use of micro-heat pipes for enhanced heat transfer is becoming more common, the exact nature of liquid evaporation from the corners of a micro-heat pipe and the associated capillary pumping capacity has not been investigated in detail. The analytical model of micro-heat pipes is necessary for the complete understanding of the transport processes and the design of such devices.

Cotter [1] first proposed the concept of micro-heat pipe as a wickless heat pipe for uniform heat distribution in electronic chip. The micro-grooved heat pipe is filled with a working fluid and the pipe is sealed. Heat flux is applied to a portion of the heat pipe, called evaporative section, to vaporize the liquid in that region. The

vapor is pushed towards the condenser section. The capillary pressure and the temperature difference between the evaporative and condenser sections promote the flow of the working fluid from the condenser back to the evaporator through the corner regions. Suman and Hoda [2] showed that the sharp angled corners are necessary for a good heat pipe operation. Swanson and Herdt [3] showed that the meniscus recession in the evaporative section causes a reduction in the meniscus radius causing an increase in the capillary pressure. The flow of fluid is primarily governed by the pressure difference at the liquid–vapor interface. The pressure difference at the interface is a function of the radius of curvature of the liquid meniscus, surface tension and wettability of the coolant liquid and substrate system [4–13].

Micro-heat pipes, which could be embedded directly onto the silicon substrate of an integrated circuit, have been investigated in several studies conducted by Mallik and Peterson [14], Mallik et al. [15] and Peterson et al. [16]. They have also reported experimental data taken on several water-charged micro-heat pipes with a cross-sectional dimension of about one millimeter. Babin et al. [17] have developed a steady-state micro-heat pipe model to quantify heat transport capacity. Longtin [18] has developed a one-dimensional steady-state model of the evaporative and adiabatic sections of a micro-heat pipe to calculate working fluid pressure, velocity and film thickness along the length of the pipe. Peterson and his co-workers [19,20] have successfully used the Young–Laplace equation to describe the internal fluid dynamics of micro-heat pipes. The minimum meniscus radius and maximum heat transport in triangular grooves have also been studied [20]. A detailed thermal analysis and various limitations of a micro-heat pipe have been done by Khrustalev and Faghri [21]. Xu and Carey [22] have developed an analytical model for evaporation from a V-shaped micro-groove surface assuming that the evaporation takes place only from the thin film region of the meniscus. Ravikumar and DasGupta [23] have presented a model for evaporation from V-shaped micro-grooves. Later, researchers have investigated the concept of using micro-heat pipe as an effective heat spreader [24,25]. Determination of dry-out length of a micro-heat pipe has also been investigated [26,27]. Catton and Stores [28] presented one-dimensional semi-analytical model for the prediction of wetted length in inclined triangular capillary groove. They have introduced the concept of accommodation theory for change in the radius of curvature at the liquid–vapor interface. Suman et al. [29] have presented a generalized model of a micro-grooved heat pipe of polygonal shape. They have performed detailed study of triangular and rectangular heat pipes. Suman et al. have also presented semi-transient modeling of a micro-grooved heat pipe of polygonal shape [30] and transient analysis of a V-shaped micro-heat pipe [31]. Technical issues related to micro-heat pipes investigated so far include liquid distribution and charge optimization by Duncan and Peterson [33] and Mallik and Peterson [34,35], interfacial thermodynamics in micro-heat pipe capillary structures by Swanson and Peterson [36,37] and micro-heat pipe transient behavior by Wu et al. [38]. Peterson [39] and Cao and Faghri [40] have done reviews of the literature on micro-heat pipes.

In the present study, the coupled nonlinear governing equations for fluid flow, heat transfer and mass transfer developed for a general model of a micro-grooved heat pipe of any polygonal shape have been solved analytically. The axial flow of the liquid as a result of the change in the radius of curvature has been modeled. The expressions for radius of curvature, liquid velocity, vapor velocity, liquid pressure, evaporative heat flux, critical heat input, dry-out length and available capillary head have been derived. The results predicted by the model have been successfully compared with the published results in literature.

2. Theory

The system in the present study consists of axially grooved-micro-heat pipe with grooves of any polygonal shape. Though the model equations in terms of the shape of the grooves are general in nature, an equilateral triangular and a rectangular heat pipe have been studied as test cases. The liquid is pushed from the cold end to the hot end due to decrease in the radius of curvature caused by the intrinsic meniscus receding into the corner. The liquid flows along the corners and the vapor passes through the open space (Fig. 1). The hot end and the cold end denote the farthest end of the evaporative and the condenser sections respectively. Decrease in the radius of curvature results decreases the liquid pressure, which is the driving force for the flow. The liquid film gradually becomes thinner and more curved (lower radius of curvature) as the liquid recedes further towards the apex of the corner.

It has been shown earlier [23] that the axial flow is primarily caused by capillary forces. The capillary forces are directly proportional to surface tension of the liquid and inverse of the radius of curvature. The radius of curvature of the liquid film is a function of the axial distance from the cold end. The model presented develops the governing equations for fluid flow and heat transfer and relates them to the capillary forces present in the system. The model equations are developed for all the three sections i.e., evaporative, adiabatic and condenser encompassing the complete heat pipe.

The governing model equations are derived with the following assumptions: (i) one dimensional steady incompressible flow along the length of heat pipe; (ii) uniform distribution of heat input; (iii) negligible heat

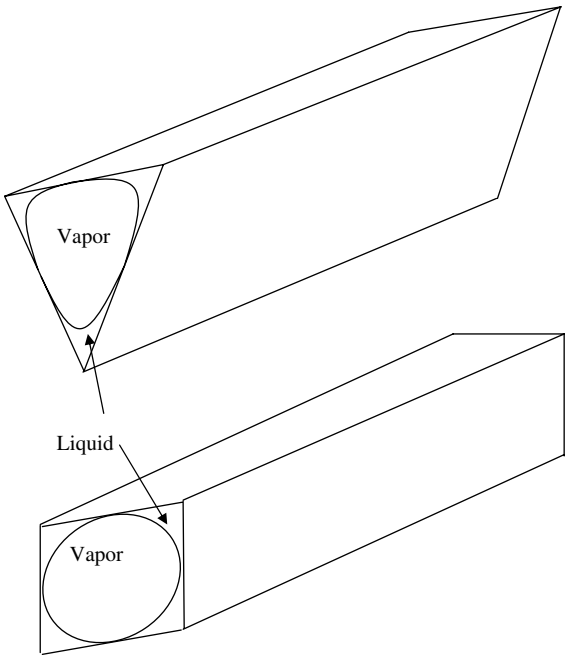

Fig. 1. Schematic of the triangular and the rectangular heat pipes.

dissipation due to viscosity; (iv) constant pressure in the vapor region in the operating range of temperature; (v) one dimensional temperature variation along the length of heat pipe; (vi) negligible shear stress at the liquid vapor interface.

The radius of curvature (R) at the cold end is a constant, which can be calculated from the geometry of the groove since the cold end is completely filled i.e. $R = R_0$ at the cold end. It is presented in the Appendix A. The evaluation of relevant geometrical parameters for different polygonal shape is also presented in Appendix A. One corner of a section of heat pipe of any polygonal shape of length Δx is shown in Fig. 2. The radius of curvature, liquid velocity and pressure vary along the length of the heat pipe. The wall shear stress (τ_w) acts against the flow of the liquid.

The steady-state momentum balance in differential form is given as

$$\rho_l A_l V_l \frac{d(V_l)}{dx} + A_l \frac{dP_l}{dx} + 2L_h \tau_w + \rho_l g \sin(\beta) A_l = 0 \qquad (1)$$

The first term in the above equation is the convective momentum change, the second term is the pressure force acting on the volume element, the third term is the wall shear force and the fourth term is gravitational force. Eq. (1) is valid for all three regions, namely evaporative, adiabatic and condensing regions. The contribution of the convective term has been found to be negligible using the order of magnitude analysis. It has also been shown [41] that the effect of gravity is negligible and heat pipes are widely used at places where gravity is not important. Therefore, after neglecting convective and gravity terms Eq. (1) can be written as

$$A_l \frac{dP_l}{dx} + 2L_h \tau_w = 0 \qquad (2)$$

The liquid pressure can be estimated from the Young–Laplace equation as

$$P_l - P_{vo} = -\frac{\sigma}{R} \qquad (3)$$

where P_l is the liquid pressure, P_{vo} is the pressure in the vapor region and R is the radius of curvature of liquid meniscus at any location, x.

The liquid velocity can be given as

$$\left.\begin{aligned} V_l &= \frac{\int_0^x W_b Q'_c(\zeta) d\zeta}{\rho_l \lambda A_l} && \text{in condensing section} \\ V_l &= \frac{Q}{\rho_l \lambda A_l} && \text{in adiabatic section} \\ V_l &= \frac{\int_x^L W_b Q'_e(\zeta) d\zeta}{\rho_l \lambda A_l} && \text{in evaporative section} \end{aligned}\right\} \qquad (4)$$

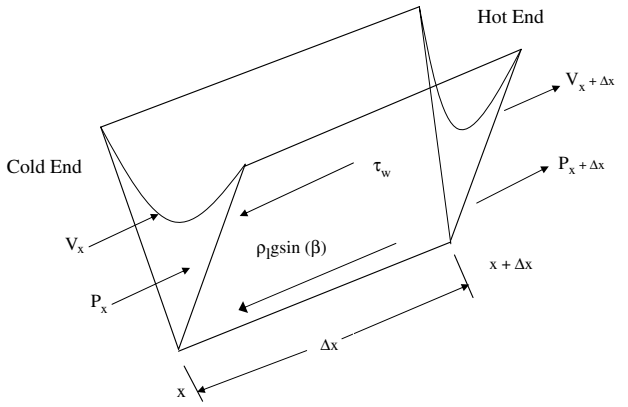

Fig. 2. Volume element of one corner of the polygon with all forces specified.

where W_b is perimeter of the polygon. Q'_c is the heat flux in the condensing section, which is negative. Q is the total heat input to the heat pipe. Q'_e is the heat flux in the evaporative section, which is positive. Eq. (3) is derived by writing the mass balances in all the three sections.

Similarly, the vapor velocity can be given as

$$\left.\begin{array}{ll} V_g = \dfrac{\int_0^x W_b Q'_c(\zeta)\mathrm{d}\zeta}{\rho_g\lambda(A_{cs}-A_l)} & \text{in condensing section} \\ V_g = \dfrac{Q}{\rho_g\lambda(A_{cs}-A_l)} & \text{in adiabatic section} \\ V_g = \dfrac{\int_x^L W_b Q'_e(\zeta)\mathrm{d}\zeta}{\rho_g\lambda(A_{cs}-A_l)} & \text{in evaporative section} \end{array}\right\} \quad (5)$$

The supplied heat raises the temperature of the liquid packet and also evaporates the liquid. Ravikumar and DasGupta [23] showed that the sensible heat content is very small as compared to the latent heat for vaporization and condensation. Hence, the sensible heat content can be neglected. Thus, the energy balance in the volume element can be expressed as

$$\left.\begin{array}{ll} Q_v = -\dfrac{Q'_c W_b}{R_l} & \text{in condensing section} \\ Q_v = 0 & \text{in adiabatic section} \\ Q_v = \dfrac{Q'_e W_b}{R_l} & \text{in evaporative section} \end{array}\right\} \quad (6)$$

The steady-state energy balance in the substrate is given by

$$\left.\begin{array}{ll} A_{cs}K_s\dfrac{\mathrm{d}^2T_s}{\mathrm{d}x^2} - Q'_c(x)W_b = 0 & \text{in condensing section} \\ A_{cs}K_s\dfrac{\mathrm{d}^2T_s}{\mathrm{d}x^2} = 0 & \text{in adiabatic section} \\ A_{cs}K_s\dfrac{\mathrm{d}^2T_s}{\mathrm{d}x^2} - Q'_e(x)W_b = 0 & \text{in evaporative section} \end{array}\right\} \quad (7)$$

where the first term is the net change in the conductive heat in the control volume and the second term is the heat taken up by the coolant liquid.

2.1. Boundary conditions

The radius of curvature of the liquid meniscus at the cold end ($x = 0$), R_0 is a constant since the cold end is completely filled. It can be obtained from the geometry for a known contact angle system. Its calculation has been presented in Appendix A.

$$\text{At} \quad x = 0, \quad R = R_0, \quad T_s = T_{con}$$

$$\text{At} \quad x = f_1 L, \quad \left.\frac{\mathrm{d}T_s}{\mathrm{d}x}\right|_{x=f_1L} = 0$$

$$\text{At} \quad x = f_2 L, \quad \left.\frac{\mathrm{d}T_s}{\mathrm{d}x}\right|_{x=f_2L} = 0$$

$$\text{At} \quad x = L, \quad Q_{in} = -K_s A_{cs}\left.\frac{\mathrm{d}T_s}{\mathrm{d}x}\right|_{x=L}$$

2.2. Nondimensionalization

Eqs. (2)–(7) are nondimensionalized using the following expressions: friction factor, $f = K'/N_{Re}$ hydraulic diameter, $D_h = 4A_l/(2L_h)$, Reynolds number, $N_{Re} = D_h\rho_l V_l/\mu$, wall shear stress, $\tau_w = \rho V^2 f/2$, reference velocity, $V_R = Q/(\rho R_0^2\lambda)$, reference pressure, $P_R = \sigma/R_0$, reference temperature, $T_R = T_{con}$. The dimensionless parameters are defined as follows: R^* (dimensionless radius of curvature) $= R/R_0$, X^* (dimensionless position) $= x/L$, V_l^* (dimensionless liquid velocity) $= V_l/V_R$, V_g^* (dimensionless vapor velocity) $= V_g/V_R$, P_l^* (dimensionless liquid pressure) $= P_l/P_R$, T_s^* (dimensionless substrate temperature) $= T_s/T_R$. K' is used in the expression of friction factor (f) and is a constant for a specific geometry (13.33 for triangle and 15.55 for rectangle with side ratio 1:2, [32,42]). R_0 is the radius of curvature at the cold end and is a function of side length, contact angle for the substrate–coolant system, and apex angle of the polygon. After nondimensionalization and rearranging, Eqs. (2), (3) and (7) can be written as

$$\frac{\mathrm{d}R^*}{\mathrm{d}X^*} = \frac{-B_2 V_R V_l^* L}{\sigma R_0} \quad (8)$$

where

$$B_2 = \frac{\mu K' \cos^2(\alpha+\gamma)}{2\sin^2\alpha\left[\dfrac{\cot(\alpha+\gamma)\cos(\alpha+\gamma)\sin\gamma}{\sin\alpha} + \{\cot(\alpha+\gamma) - \varphi/2\}\right]^2}$$

Its derivation has been presented in Appendix A.

$$P_l^* = \frac{P_{vo}}{P_R} - R^* \quad (9)$$

$$\left.\begin{array}{ll} \dfrac{\mathrm{d}^2T_s^*}{\mathrm{d}X^{*2}} - \dfrac{Q'_c(X^*)W_b L^2}{T_R A_{cs} K_s} = 0 & \text{in condensing section} \\ \dfrac{\mathrm{d}^2T_s}{\mathrm{d}X^{*2}} = 0 & \text{in adiabatic section} \\ \dfrac{\mathrm{d}^2T_s^*}{\mathrm{d}X^{*2}} - \dfrac{Q'_e(X^*)W_b L^2}{T_R A_{cs} K_s} = 0 & \text{in evaporative section} \end{array}\right\} \quad (10)$$

The dimensionless boundary condition can be written as

$$\text{at} \quad X^* = 0, \quad R^* = 1, \quad T_s^* = 1$$

$$\text{at} \quad X^* = f_1, \quad \left.\frac{\mathrm{d}T_s^*}{\mathrm{d}X^*}\right|_{X^*=f_1} = 0$$

$$\text{at} \quad X^* = f_2, \quad \left.\frac{\mathrm{d}T_s^*}{\mathrm{d}X^*}\right|_{X^*=f_2} = 0$$

$$\text{at} \quad X^* = 1, \quad Q_{in} = -\frac{K_s A_{cs} T_R}{L}\left.\frac{\mathrm{d}T_s^*}{\mathrm{d}X^*}\right|_{X^*=1}$$

Using above boundary condition, the variations of dimensionless radius of curvature can be obtained if the expression for V_l^* is known. The temperature profile

of the substrate can be obtained analytically using Eq. (10) and the above boundary conditions since the evaporative and condensing heat fluxes are function of position. The expressions for liquid velocity, vapor velocity, dimensionless radius of curvature, liquid pressure and evaporative heat flux for all three sections have been presented in next sections.

2.2.1. The condensing section

$$V_l^* = \frac{\int_0^{X^*} W_b Q_c'(\eta)\mathrm{d}\eta}{V_R \rho_l \lambda A_l} \tag{11}$$

$$V_g^* = \frac{\int_0^{X^*} W_b Q_c'(\eta)\mathrm{d}\eta}{V_R \rho_g \lambda (A_{cs} - A_l)} \tag{12}$$

$$R^* = \sqrt[3]{1 - 3B_1' \int_0^{X^*} \left\{ \int_0^{\eta} Q_c'(\xi)\mathrm{d}\xi \right\} \mathrm{d}\eta} \tag{13}$$

where

$$B_1' = \frac{B_2 L^2 W_b}{\sigma R_0^3 \rho_l \lambda B_1}$$

$$P_l^* = \frac{P_{vo}}{P_R} - \sqrt[3]{1 - 3B_1' \int_0^{X^*} \left\{ \int_0^{\eta} Q_c'(\xi)\mathrm{d}\xi \right\} \mathrm{d}\eta} \tag{14}$$

$$Q_v = -\frac{Q_c' W_b}{R_l} \tag{15}$$

2.2.2. The adiabatic section

$$V_l^* = \frac{Q}{V_R \rho_l \lambda A_l} \tag{16}$$

$$V_g^* = \frac{Q}{V_R \rho_g \lambda (A_{cs} - A_l)} \tag{17}$$

$$R^* = \sqrt[3]{(R_1^*)^3 - 3QB_2'(X^* - f_1)} \tag{18}$$

where

$$R_1^* = R^*(f_1) = \sqrt[3]{1 - 3B_1' \int_0^{f_1} \left\{ \int_0^{\eta} Q_c'(\xi)\mathrm{d}\xi \right\} \mathrm{d}\eta}$$

and

$$B_2' = \frac{B_2 L}{\sigma R_0^3 \rho_l \lambda B_1}$$

$$P_l^* = \frac{P_{vo}}{P_R} - \sqrt[3]{(R_1^*)^3 - 3QB_2'(X^* - f_1)} \tag{19}$$

$$Q_v = 0 \tag{20}$$

2.2.3. The evaporative section

$$V_l^* = \frac{\int_0^{X^*} W_b Q_e'(\eta)\mathrm{d}\eta}{V_R \rho_l \lambda A_l} \tag{21}$$

$$V_g^* = \frac{\int_0^{X^*} W_b Q_c'(\eta)\mathrm{d}\eta}{V_R \rho_g \lambda (A_{cs} - A_l)} \tag{22}$$

$$R^* = \sqrt[3]{(R_2^*)^3 - 3B_3' \int_{f_2}^{X^*} \left\{ \int_{\eta}^{1} Q_e'(\xi)\mathrm{d}\xi \right\} \mathrm{d}\eta} \tag{23}$$

where

$$R_2^* = R^*(f_2) = \sqrt[3]{(R_1^*)^3 - 3B_2'(X^* - f_1)}$$

and

$$B_3' = \frac{B_2 L^2 W_b}{\sigma R_0^3 \rho_l \lambda B_1} = B_1'$$

$$P_l^* = \frac{P_{vo}}{P_R} - \sqrt[3]{(R_2^*)^3 - 3B_3' \int_0^{X^*} \left\{ \int_0^{\eta} Q_e'(\xi)\mathrm{d}\xi \right\} \mathrm{d}\eta} \tag{24}$$

$$Q_v = \frac{Q_e' W_b}{R_l} \tag{25}$$

2.3. Critical heat input and dry-out length

The value of R^* at the hot end can predict the maximum heat input for the system known as the operating limit or the critical heat input of the heat pipe. The critical heat input is defined as the heat input for which the flow due to the curvature change is not able to meet the requirement of fluid evaporation at the hot end i.e. sufficient coolant fluid is not available for evaporation at the hot end. For critical heat input, as no fluid is available for evaporation, the radius of curvature of the liquid meniscus at the hot end reaches a value very close to zero. Then, the device approaches its operating limit. Therefore, any heat input higher than the critical heat input propagates the dry region starting from the hot end towards the cold end. Based on this principle, the expressions for the critical heat input and the dry-out length have been developed.

The critical heat input is the heat input for which the radius of curvature (R^*) of the liquid meniscus at the hot end ($X^* = 1$) reaches a value very close to zero and the device approaches its operating limit. Mathematically, this can be represented as follows:

For $Q = Q_{cr}$, $R^* = 0$ at $X^* = 1$

Hence, by solving Eqs. (13), (18) and (23) for known heat flux distributions in evaporative and condensing sections, the expression for the critical heat input can be obtained. By taking constant heat fluxes in evaporative and condensing regions ($Q_c' = \frac{Q}{f_1 W_b L}$ and $Q_e' = \frac{Q}{(1-f_2) W_b L}$), the expression for the critical heat input can be given as follows:

$$Q_{cr} = \frac{2B_1 \sigma \rho_l \lambda R_0^3}{3B_2 L\{1 + f_2 - f_1\}} \tag{26}$$

By taking $Q_c' = \frac{Q(m+1)}{W_b (f_1 L)^{m+1}} (f_1 - X^*)^m$ and $Q_e' = \frac{Q(m+1)}{W_b (L(1-f_2))^{m+1}} \times (X^* - f_2)^m$, the expression for critical heat input is obtained as

$$Q_{cr} = \frac{\sigma\rho_1\lambda B_1 (R_0)^3}{3B_2L(f_2 - f_1) + \frac{3B_2L(1 - f_2 + f_1)}{L^m}\left(\frac{m+1}{m+2}\right)} \quad (27)$$

The analytical model presented here can be used to calculate the dry-out length (L_d) for a set of process variables. The radius of curvature at the hot end for the critical heat input becomes very close to zero. The capillary pumping becomes less than the rate of evaporation for heat input higher than the critical heat. This propagates the dry region starting from the hot end towards the cold end. The dry region of the heat pipe is known as dry-out length. If $Q < Q_{cr}$, the heat pipe is working without generating any dry-region. If the heat input is greater than the critical heat input and less than the heat required (Q_2) to onset the dry-out at the junction of the evaporative and the adiabatic sections i.e. $R_2^* = 0$, the dry-out region is only in the evaporative section. The general expression for Q_2 can be obtained by equating R_2^* to zero as follows:

$$3B_2'(f_2 - f_1) = 1 - 3B_1' \int_0^{f_1} \left\{ \int_0^{\eta} Q'(\xi)\mathrm{d}\xi \right\} \quad (28)$$

The dry-out length can be calculated by evaluating X_d^* as follows:

$$3B_3' \int_{f_2}^{X_d^*} \left\{ \int_{\eta}^{1} Q'(\xi)\mathrm{d}\xi \right\} \mathrm{d}\eta = R_2^3 \quad (29)$$

and

$$L_d = L(1 - X_d^*) \quad (30)$$

For the constant heat input distributions in evaporative and condensing sections, the expressions for Q_2 and the dry-out length can be given as follows:

$$Q_2 = \frac{\sigma B_1\rho_1\lambda R_0^3}{3B_2L\left\{(f_2 - f_1) + \frac{(f_1)^2}{2(1 - f_2)}\right\}} \quad (31)$$

$$L_d = L\sqrt{1 - 2\left\{\frac{(R_2^*)^3(1 - f_2)\sigma B_1 R_0^3\rho_1\lambda}{3B_2LQ} + f_2 - \frac{(f_2)^2}{2}\right\}} \quad (32)$$

If $Q_2 < Q < Q_1$ (input heat required to onset of dry-out at the junction of the adiabatic and condensing sections), the dry-region is in the evaporative and the adiabatic sections. The expression for Q_1 can be obtained by equating R_1^* to zero as

$$1 = 3B_1' \int_0^{f_1} \left\{ \int_0^{\eta} Q'(\xi)\mathrm{d}\xi \right\} \mathrm{d}\eta \quad (33)$$

The expression for the dry-out length can be obtained using Eq. (30) where X_d^* is given as follows:

$$X_d^* = \frac{R_1^3}{3B_2'} + f_1 \quad (34)$$

For constant heat input distributions in evaporative and condensing sections, the expressions for Q_1 and the dry-out length are given as follows:

$$Q_1 = \frac{2B_1\sigma R_0^3\rho_1\lambda}{3B_2Lf_1} \quad (35)$$

$$L_d = L\left(1 - \frac{(R_1^*)^3}{3B_2'} + f_1\right) \quad (36)$$

If $Q > Q_1$, the dry-out is in all three sections and it is calculated using Eq. (30) where X_d^* is given as follows:

$$3B_1' \int_0^{X_c^*} \left\{ \int_0^{\eta} Q'(\xi)\mathrm{d}\xi \right\} \mathrm{d}\eta = 1 \quad (37)$$

For constant heat input distribution, the expression for dry-out is given as follows:

$$L_d = L\left(1 - \sqrt{\frac{2B_1\sigma R_0^3\rho_1\lambda}{3B_2Lf_1}}\right) \quad (38)$$

2.4. Available capillary head

Capillary pumping is the driving force for fluid flow in a micro-heat pipe. Therefore, it is useful to know the available capillary head for fluid flow. Using the analytical model, the expression for the available capillary head for fluid flow is given as

$$H_c = \sigma\left\{\frac{1}{R^*(1)} - \frac{1}{R^*(0)}\right\} = \frac{\sigma}{\sqrt[3]{1 - 3B_1'\int_0^{f_1}\left\{\int_0^{\eta} Q'(\xi)\mathrm{d}\xi\right\}\mathrm{d}\eta - 3B_2'(f_2 - f_1) - 3B_3'\int_{f_2}^{1}\left\{\int_{\eta}^{1} Q'(\xi)\mathrm{d}\xi\right\}\mathrm{d}\eta}} \quad (39)$$

For the constant heat input in evaporative and condensing sections, the expression for the available capillary head becomes

$$H_c = \frac{\sigma}{\sqrt[3]{1 - \frac{3B_2LQ(f_1 - f_2 + 1)}{2\sigma\rho_1\lambda B_1 (R_0)^3}}} \quad (40)$$

3. Results and discussion

Two test cases are analyzed and the model is validated with the numerical results of Suman et al. [29]

and experimental result of Anand et al. [27]. The heat pipes selected for this study are: (i) an equilateral triangular heat pipe with side equal to 400 μm and (ii) a rectangular (400 μm × 800 μm) heat pipe. The model is also valid for any regular polygon with number of sides greater than four. Pentane is the working fluid with silicon as the substrate. Pentane wets silicon completely i.e. contact angle (γ) is zero. The origin of the coordinate system is at the cold end ($X^* = 0$). In the subsequent figures, Tr and Re are used to denote triangular and rectangular heat pipes, respectively.

The radius of curvature has an important role in the performance of micro-heat pipes. The profiles of the dimensionless radius of curvature along the length of the heat pipe (R^* vs. X^*) obtained by the analytical model presented and the numerical model of Suman et al. [29] have been presented in Fig. 3. The numerical model of Suman et al. [29] is experimentally validated with a mean error percentage of 3.0%. Good agreement between the profiles obtained by both the models has been obtained. The rate of change of the dimensionless radius of curvature is nearly constant for the triangular heat pipe. This result is in agreement with the model of Longtin et al. [18]. The radius of curvature at the hot end for rectangular heat pipe is more depressed than that for triangular heat pipe. With increase in the number of sides of a regular polygon, apex angle increases. Increase in the apex angle decreases the curvature at the cold end which decreases the capillary force of the working fluid. With increase in the number of sides of a regular polygon, friction factor also increases. The increase in friction factor will cause a decrease in liquid velocity which results in further decrease of the capillary capacity. Thus, the performance of a heat pipe goes down with increase in the number of sides. This is in agreement with the expressions for R^* given in Eqs. (13), (18) and (23) which suggest that the depression in liquid meniscus (decrement in R^* values between the cold end and the hot end) will be less to transport the same amount of heat if $B_2' = \frac{B_2 L}{\sigma R_0^3 \rho_l \lambda B_1}$ is less. The value of B_2' is 16.1596 and 29.444 for triangular and rectangular heat pipes, respectively. Finally, it can be concluded that a coolant liquid having less $\frac{\mu}{\sigma \rho_l \lambda}$ and less $\frac{K' L}{B_1 R_0^3}$ should be chosen to optimize the heat pipe performance.

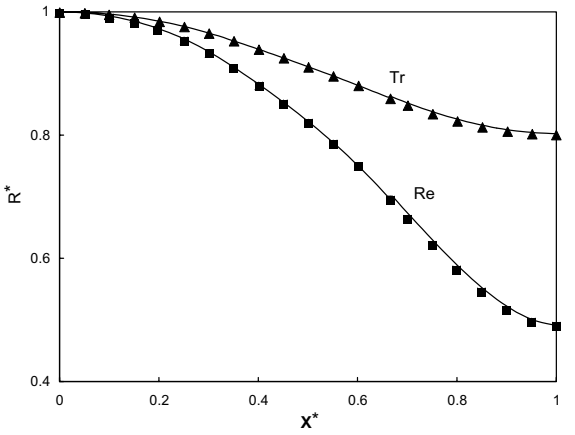

Fig. 3. Comparison between the present model and the model by Suman et al. [29] for the variation of the dimensionless radius of curvature, R^*, with dimensionless position, X^*, for triangular and rectangular heat pipes. Solid lines are with the present model and points are with Suman et al. [29] model.

The liquid velocities can be obtained from Eqs. (11), (16) and (21) and the vapor velocities can be obtained from Eqs. (12), (17) and (22) for vapor velocities. The liquid and vapor velocities decrease with increase in the latent heat of vaporization and the density. If $B_2' = \frac{B_2 L}{\sigma R_0^3 \rho_l \lambda B_1}$ is less, depression in liquid meniscus is less and therefore, liquid velocity is less as more area is available for liquid flow.

The evaporative heat flux can be obtained by using Eqs. (15), (20) and (25). If $B_2' = \frac{B_2 L}{\sigma R_0^3 \rho_l \lambda B_1}$ is less, the evaporative heat flux is less. Therefore, the capillary pressure required is also less, which is supported by Eqs. (14), (19) and (22).

By solving Eqs. (13), (18) and (23), the critical heat input can be obtained using $R^* = 0$ at $X^* = 1$. The expressions for the critical heat input taking constant and variable heat input distributions in evaporative and condensing sections is given by Eqs. (26) and (27). The expression shows that the critical heat input can be increased by increasing the surface tension, the latent heat of vaporization, the liquid density, side length and by decreasing the groove angle, the length of heat pipe, the length of adiabatic section (which is a heat transportation section), and the viscosity. Eq. (26) is also in agreement with the model of Longtin et al. [18] which shows that the maximum heat transport capacity of a micro-heat pipe varies with the inverse of its length and the cube of its side length. The critical heat inputs for the triangular and the rectangular heat pipes obtained by the model presented and the model of Suman et al. [29], which is experimentally validated, have been presented in Table 1. Good agreement between the critical heat inputs obtained by both the models has been observed. Additionally, the ratio of critical heat inputs for triangular and rectangular heat pipes is obtained as 1.822, which approximately matches with the value 1.6 as reported by Moon et al. [42]. The difference between the two values might be due to less sharp grooves in their work. The value of critical heat input is more for triangular heat pipe than that for rectangular heat pipe. This is due to the geometrical parameter, $\frac{B_1 R_0^3}{B_2}$, in the expression of the critical heat input. Its values for triangular and rectangular heat pipes are 3.7284E−10 and 2.0606E−10 respectively. Though the values of B_2 are 0.008478 and 0.03354 for triangular and rectangular

Table 1
Variation of the critical heat input, Q_{cr} (W) with number of sides of polygonal heat pipes of length 2 cm by the model presented and the model by Suman et al. [29]

Number of sides (n)	Q_{cr}, present model (W)	Q_{cr}, Suman et al. [29] (W)
3	0.03102	0.03101
4	0.01702	0.01701

heat pipes respectively and the values of $B_1R_0^3$ are 3.161E−12 and 6.8635E−12 for rectangular and triangular heat pipes respectively. Further, Eqs. (26) and (27) suggest that the critical heat input decreases with increase in groove apex angle since the value of B_2 increases and the effect of B_2 dominates the opposing effect of $B_1R_0^3$.

The presented analytical model is capable of calculating dry-out length. The value of location, where R^* is zero gives the onset of dry-out length and the region beyond that location towards the hot end is dry. The length of dry-region is termed as dry-out length. Using this methodology, the expression for dry-out length has been presented. The expressions for dry-out length for the constant heat input distributions in evaporative and condenser sections have been given in Eqs. (32), (36) and (38). The dry-out lengths for the triangular and the rectangular heat pipes obtained by the model presented and the model of Suman et al. [29], which is experimentally validated, have been presented in Fig. 4. Good agreement between the dry-out lengths obtained by both the models has been observed. The dry-out length for triangular heat pipe is less than that for rectangular heat pipe and their difference decreases with the increase in heat input. This is due to the geometrical parameter, $\frac{B_1R_0^3}{B_2}$, in the expression of the dry-out length. With the increase in heat input, effect of the geometrical parameter on the dry-out length decreases and therefore, the difference in dry-out length between rectangular and triangular heat pipes decreases.

The fluid flow in the micro-heat pipe is because of capillary pumping. Therefore, the estimation of the capillary pressure generated is an important parameter of micro-heat pipe. Analytical expression for the available capillary head has been presented in Eq. (39). For the constant heat input distributions in evaporative and condensing sections, the value for the capillary heat available for the fluid flow is given by Eq. (40). It is seen that a coolant liquid with higher surface tension, latent heat of vaporization and density, and lower viscosity, more capillary head will be available for flow.

In all the above sections, it can be seen that B_2' plays an important role to predict the performance of a micro-heat pipe. It can be nondimensionlized using the heat input, Q_{in} as $B = \frac{1}{B_2'Q_{in}}$ and B can be called as the performance factor of a micro-heat pipe. Higher the value of B, better is the performance. The values of performance factor of triangular and rectangular heat pipes for a heat input of 0.015 W are 4.1254 and 2.2641 respectively. Based on above observation, it is suggested that the value of B should be calculated while designing a micro-heat pipe. Thus, a combination of thermophysical properties of the coolant liquid, design parameters and contact angle of the liquid–substrate system that gives higher value of B should be chosen for a fixed heat input.

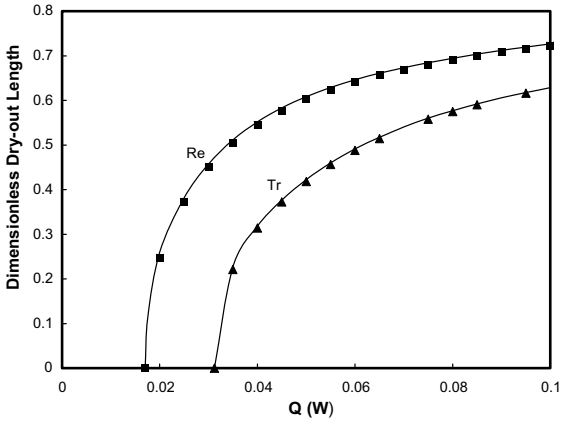

Fig. 4. Comparison between the present model and the model by Suman et al. [29] for the variation of the dimensionless dry-out length, with heat input, Q (W), for triangular and rectangular heat pipes. Solid lines are with the present model and points are with Suman et al. [29] model.

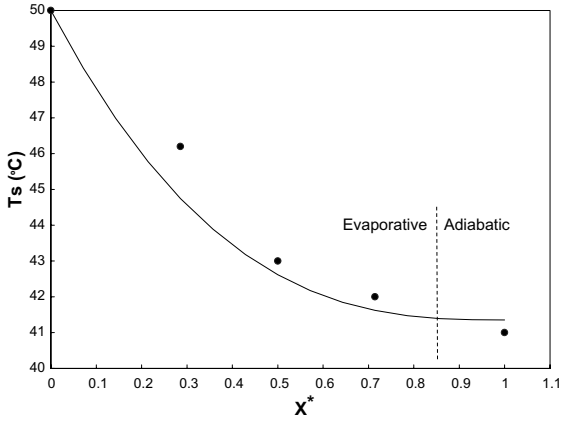

Fig. 5. Comparison between the present model and experimental results by Anand et al. [27] for the variation of the substrate temperature, with dimensionless position, X^*, for $Q = 1.52$ W and inclination angle = 0°. Solid lines are with the present model and points are with Anand et al. [27] model.

By solving Eq. (10) with the given boundary conditions, temperature profile of the substrates can be obtained. The obtained temperature profile of the substrate for the value of Q as 1.52 W and inclination angle of 0° has been compared with the experimental results of Anand et al. [27] in Fig. 5. In Anand et al. [27], experiments were carried out in a specially designed cell to study the onset and propagation of dry out point on a micro-grooved silicon surface (0.8 cm × 2.8 cm) with pentane as the coolant liquid. 33 V-grooves of 2 cm length and 100 μm wide with groove depth of 68.82 μm were used together with a groove pitch of 200 μm. A series of small thermocouples accurately measured the temperature profiles as functions of heat input to the system and inclination angle. Here, the evaporative length of 7 mm has been considered for the comparison as beyond that length the temperature is almost constant, which is considered as adiabatic section. For the comparison, the heat flux in the evaporative section, $Q'_e = \frac{Q(m+1)}{W_b(L(1-f_2))^{m+1}}(X^* - f_2)^m$ with a value of m as 0.78 has been considered. The obtained results are in good agreement with the experimental temperature profile of the substrate for wet run obtained by Anand et al. [27] and the maximum difference between experimental and analytical result is 1.45 °C. The obtained temperature is higher in adiabatic section since convective heat loss is neglected and is higher in adiabatic section since in this study no heat transfer between the substrate and coolant liquid is considered though it is not the case in real situation.

4. Conclusions

A simple generalized analytical model for fluid flow and heat transfer in a micro-heat pipe of polygonal shape has been developed by utilizing a macroscopic approach. Two different heat pipes of triangular and rectangular shape have been considered for the present study. The analytical expressions for liquid velocity, vapor velocity, dimensionless radius of curvature, liquid pressure and evaporative heat flux, critical heat input, dry-out length and available capillary head have been developed. Effect of physical properties, design parameters, etc. can be studied using this model. The analytical model gives quantitative measurement for associated fluid flow and heat transfer parameters. The model calculates the performance factor, which is useful to design such a device. Higher is the value of performance factor; better is the performance of the heat pipe, i.e. higher critical heat input. The analytical nature of the model makes it more useful and easy to use. The model is validated with the published results from literature and good agreement has been obtained. The present study can be further extended to two-dimensional variation in heat transfer, fluid flow and radius of curvature.

Appendix A

For polygonal heat pipe with equal sides

$$R_0 = \frac{a\sin\alpha}{2\cos(\alpha+\gamma)}$$

where a is side length of the polygon or smaller side of the rectangle.

$$Q' = Q_{in}/naL$$

where Q_{in} is the heat input and Q' is the heat flux.

$$\alpha = (n-2)\pi/2n$$

where α is half apex angle and n is the number of sides of the polygon.

$$W_b = na$$

where W_b is groove perimeter.

For the rectangular heat pipe (side ratio 1:2)

$$R_0 = \frac{a\sin\alpha}{2\cos(\alpha+\gamma)}$$

$$Q' = \frac{Q_{in}}{2(a+a_1)L}$$

where a_1 is the larger side of rectangle.

$$\alpha = \pi/4$$

$$W_b = 2(a+a_1)$$

For the triangular (equilateral) heat pipe

$$R_0 = \frac{a\sin\alpha}{2\cos(\alpha+\gamma)}$$

$$Q' = \frac{Q_{in}}{3aL}$$

$$\alpha = \pi/6$$

$$W_b = 3a$$

Geometry of one corner of the polygonal heat pipe is presented in Fig. A1.

The shaded area in Fig. A1 is the cross-sectional area of the liquid in the heat pipe. The cross-section area of one corner is expressed as

$$A'_1 = \text{Area of ACBD} + \text{Area of } \Delta\text{ABC} - (\text{Area of sector AOB} - \text{Area of } \Delta\text{AOB})$$

The line diagram of section OBC in Fig. A1 is presented in Fig. A2 in detail.

From Fig. A2, AC and BC are the tangents to the liquid meniscus

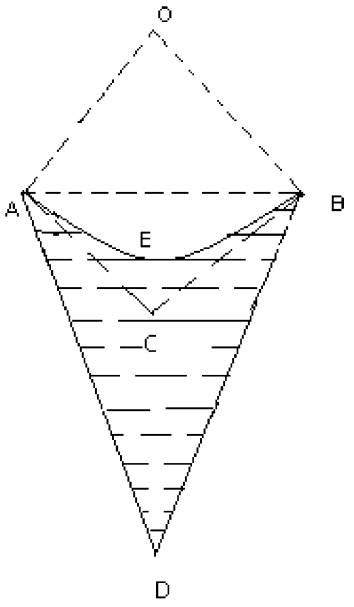

Fig. A1. Geometry of a liquid filled corner.

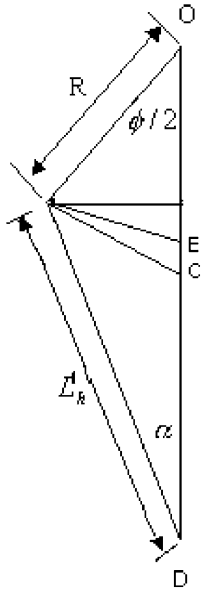

Fig. A2. Line diagram of section OBD in Fig. A1.

$\angle \mathrm{ACD} = \gamma$

$\angle \mathrm{ADC} = \alpha$

$\angle \mathrm{ACB} = 2(\alpha + \gamma)$

$\angle \mathrm{AOB} = \phi = \pi - 2(\alpha + \gamma)$

$$L_{\mathrm{h}}' = R\frac{\cos(\alpha+\gamma)}{\sin\alpha}$$

$L_{\mathrm{h}} = nL_{\mathrm{h}}'$

$R_{\mathrm{l}} = nR\phi$

$$\text{Area of ACBD} = \frac{R^2\cot(\alpha+\gamma)\cos(\alpha+\gamma)\sin\gamma}{\sin\alpha}$$

$$\text{Area of } \Delta\mathrm{ABC} = R^2\cot(\alpha+\gamma)\cos^2(\alpha+\gamma)$$

$$\text{Area of sector AOB} = \phi R^2/2$$

$$\text{Area of } \Delta\mathrm{AOB} = R^2\cos(\alpha+\gamma)\sin(\alpha+\gamma)$$

Hence

$$A_1' = R^2\left[\{\cot(\alpha+\gamma) - \varphi/2\} + \frac{\cot(\alpha+\gamma)\cos(\alpha+\gamma)\sin\gamma}{\sin\alpha}\right]$$

and

$$\begin{aligned} A_1 &= nA_1' \\ &= nR^2\left[\{\cot(\alpha+\gamma) - \varphi/2\} + \frac{\cot(\alpha+\gamma)\cos(\alpha+\gamma)\sin\gamma}{\sin\alpha}\right] \\ &= B_1R^2, \end{aligned}$$

where

$$B_1 = n\left[\{\cot(\alpha+\gamma) - \varphi/2\} + \frac{\cot(\alpha+\gamma)\cos(\alpha+\gamma)\sin\gamma}{\sin\alpha}\right]$$

$$B_2 = \frac{\mu K'\cos^2(\alpha+\gamma)}{2\sin^2\alpha\left[\frac{\cot(\alpha+\gamma)\cos(\alpha+\gamma)\sin\gamma}{\sin\alpha} + \{\cot(\alpha+\gamma) - \varphi/2\}\right]^2}$$

References

[1] T.P. Cotter, Principles and prospects of micro-heat pipes, in: Proceedings of the 5th International Heat Pipe Conference, Tsukuba, Japan, 1984, pp. 328–332.

[2] B. Suman, N. Hoda, Effect of variations in thermophysical properties and design parameters on the performance of a V-shaped micro-grooved heat pipe, Int. J. Heat Mass Transfer 48 (2005) 2090–2101.

[3] L.W. Swanson, G.C. Herdt, Model of the evaporative meniscus in a capillary tube, J. Heat Transfer 114 (1992) 434–441.

[4] S. Das Gupta, J.A. Schonberg, I.Y. Kim, P.C. Wayner Jr., Use of augmented Young–Laplace equation to model equilibrium and evaporation extended meni-sci, J. Colloid Interface Sci. 157 (1993) 332–342.

[5] S. DasGupta, J.A. Schonberg, P.C. Wayner Jr., Investigation of an evaporative extended meniscus based on the augmented Young–Laplace equation, J. Heat Transfer 115 (1993) 201–208.

[6] M.L. Gee, T.W. Hearly, L.R. White, Ellipsometric studies of alkenes adsorption on quartz, J. Colloid Interface Sci. 131 (1) (1989) 18–23.

[7] S. Gokhale, J.L. Plawsky, P.C. Wayner Jr., S. DasGupta, Inferred pressure gradient and fluid flow in a condensing sessile droplet based on the measured thickness profile, Phys. Fluids 16 (6) (2004) 1942–1955.

[8] S. Moosman, S.M. Homsy, Evaporating menisci of wetting fluids, J. Colloid Interface Sci. 73 (1980) 212–223.

[9] F. Renk, P.C. Wayner Jr., An evaporating ethanol meniscus; Part II: analytical studies, J. Heat Transfer 101 (1979) 55–62.
[10] J.G. Troung, P.C. Wayner Jr., Effects of capillary and Vander Waals dispersion forces on the equilibrium profile of a wetting liquid: theory and experimental, J. Chem. Phys. 87 (1987) 4180–4188.
[11] P.C. Wayner Jr., The effect of interfacial mass transport on flow in thin liquid films, Colloids Surf. 52 (1991) 71–84.
[12] P.C. Wayner Jr., Y.K. Kao, L.V. LaCroix, The interline heat transfer coefficient of an evaporative wetting film, Int. J. Heat Mass Transfer 19 (1976) 487–492.
[13] L. Zheng, J.L. Plawsky, P.C. Wayner Jr., S. DasGupta, Stability and oscillations in an evaporating corner meniscus, J. Heat Transfer 126 (2004) 169–178.
[14] A.K. Mallik, G.P. Peterson, Transient response characteristics of vapor deposited micro-heat pipe, J. Electron. Pack. 117 (1995) 82–87.
[15] A.K. Mallik, G.P. Peterson, M.H. Weichold, On the use of micro-heat pipes as an integral part of semiconductor devices, J. Electron. Pack. 114 (1992) 436–442.
[16] G.P. Peterson, A.B. Duncan, M.H. Weichold, Experimental investigation of micro-heat pipes fabricated in silicon wafers, J. Heat Transfer 115 (1993) 750–756.
[17] B.R. Babin, G.P. Peterson, D. Wu, Steady-state modeling and testing of a micro-heat pipe, J. Heat Transfer 112 (1990) 595–601.
[18] J.P. Longtin, B. Badran, F.M. Gerner, A one-dimensional model of a micro-heat pipe during steady-state operation, J. Heat Transfer 116 (1994) 709–715.
[19] D. Wu, G.P. Peterson, Investigation of the transient characteristics of a micro-heat pipe, J. Thermophys. Heat Transfer 5 (1991) 129–134.
[20] G.P. Peterson, H.B. Ma, Theoretical analysis of the maximum heat transport in triangular grooves: a study of idealized micro-heat pipe, J. Heat Transfer 118 (1996) 731–739.
[21] D. Khrustalev, A. Faghri, Thermal analysis of a micro-heat pipe, J. Heat Transfer 116 (1) (1994) 189–198.
[22] X. Xu, V.P. Carey, Film evaporation from a micro-grooved surface—an approximate heat transfer model and its comparison with experimental data, J. Thermophys. Heat Transfer 4 (1990) 512–520.
[23] M. Ravikumar, S. DasGupta, Modeling of evaporation from V-shaped micro-grooves, Chem. Eng. Commun. 160 (1997) 225–248.
[24] H.B. Ma, G.P. Peterson, Experimental investigation of the maximum heat transport in triangular grooves, J. Heat Transfer 118 (1996) 740–746.
[25] A.Md. Khan, S. Mishro, S. De, S. DasGupta, An experimental and theoretical investigation of evaporating cooling from V-shaped microgrooves, Int. J. Transport Phenom. 1 (1999) 277–289.
[26] J.M. Ha, G.P. Peterson, Analytical prediction of axial dry-out point for evaporating liquids in axial microgrooves, J. Heat Transfer 120 (1998) 452–457.
[27] S. Anand, S. De, S. DasGupta, Experimental and theoretical study of axial dry-out point for evaporative from V-shaped microgrooves, Int. J. Heat Mass Transfer 45 (2002) 1535–1543.
[28] I. Catton, G.R. Stores, A semi-analytical model to predict the capillary limit of heated inclined triangular capillary grooves, J. Heat Transfer 124 (2002) 162–168.
[29] B. Suman, S. De, S. DasGupta, A model of the capillary limit of a micro-grooved heat pipe and the prediction of dry out length, Int. J. Heat Fluid Flow 26 (3) (2005) 495–505.
[30] B. Suman, S. De, S. DasGupta, Transient modeling of micro-grooved heat pipe, Int. J. Heat Mass Transfer 48 (8) (2005) 1633–1646.
[31] B. Suman, N. Hoda, An extension of the transient model of micro-grooved heat pipe, J. Heat Transfer (2005).
[32] H.Y. Wu, P. Cheng, Friction factor in smooth trapezoidal silicon microchannels with different aspect ratios, Int. J. Heat Mass Transfer 46 (2003) 2519–2525.
[33] A.B. Duncan, G.P. Peterson, Charge optimization for a triangular-shaped etched micro-heat pipe, J. Thermophys. Heat Transfer 9 (1995) 365–367.
[34] A.K. Mallik, G.P. Peterson, Steady-state investigation of vapor deposited micro-heat pipe arrays, J. Electron. Pack. 117 (1995) 75–81.
[35] A.K. Mallik, G.P. Peterson, M.H. Weichold, Fabrication of vapor-deposited micro-heat pipe arrays as an integral part of semiconductor devices, J. Electromech. Syst. 4 (1995) 119–131.
[36] L.W. Swanson, G.P. Peterson, Interfacial thermodynamics of the capillary structures in micro-heat pipes, in: F.M. Gerner, K.S. Udell (Eds.), Heat Transfer on the Micro-scale, ASME Heat Transfer Division, New York, NY, HTD 253, 1993, pp. 45–51.
[37] L.W. Swanson, G.P. Peterson, Interfacial thermodynamics of micro-heat pipes, J. Heat Transfer 117 (1995) 195–201.
[38] D. Wu, G.P. Peterson, W.S. Chang, Transient experimental investigation of micro-heat pipes, J. Thermophys. Heat Transfer 5 (1991) 129–134.
[39] G.P. Peterson, Overview of micro-heat pipe research and development, Appl. Mech. Rev. 45 (1992) 175–189.
[40] Y. Cao, A. Faghri, Micro/miniature heat pipes and operating limitations, J. Enhanced Heat Transfer 1 (3) (1994) 265–274.
[41] S.H. Moon, G. Hwang, S.C. Ko, Y.T. Kim, Experimental study on the thermal performance of micro-heat pipe with cross-section of polygon, Microelectron. Reliab. 44 (2004) 315–321.
[42] P.S. Ayyaswamy, I. Catton, D.K. Edwards, Capillary flow in triangular grooves, ASME J. Appl. Mech. 41 (2) (1974) 248–265.